Available online at www.sciencedirect.com
ScienceDirect
Journal of Solid State Chemistry 180 (2007) 2991–3000
JOURNAL OF SOLID STATE CHEMISTRY
www.elsevier.com/locate/jssc

Structures and crystal chemistry of the double perovskites $Ba_2LnB'O_6$ (Ln = lanthanide $B' = Nb^{5+}$ and Ta^{5+}): Part I. Investigation of Ba_2LnTaO_6 using synchrotron X-ray and neutron powder diffraction

Paul J. Saines[a], Jarrah R. Spencer[a], Brendan J. Kennedy[a,*], Maxim Avdeev[b]

[a]*School of Chemistry, The University of Sydney, Sydney, New South Wales 2006, Australia*
[b]*Bragg Institute, ANSTO, Private Mail Bag 1, Menai, New South Wales 2234, Australia*

Received 25 May 2007; received in revised form 5 August 2007; accepted 10 August 2007
Available online 28 August 2007

Abstract

The structure of 14 compounds in the series Ba_2LnTaO_6 have been examined using synchrotron X-ray diffraction and found to undergo a sequence of phase transitions from $I2/m$ monoclinic to $I4/m$ tetragonal to $Fm\bar{3}m$ cubic symmetry with decreasing ionic radii of the lanthanides. Ba_2LaTaO_6 is an exception to this with variable temperature neutron diffraction being used to establish that the full series of phases adopted over the range of 15–500 K is $P2_1/n$ monoclinic to $I2/m$ monoclinic to $R\bar{3}$ rhombohedral. The chemical environments of these compounds have also been investigated and the overbonding to the lanthanide cations is due to the unusually large size for the B-site in these perovskites.

Keywords: Perovskite; Phase transition; Synchrotron X-ray powder diffraction; Neutron powder diffraction

1. Introduction

The physical properties of Ba_2LnTaO_6 (Ln = lanthanides and Y^{3+}) double perovskites are of significant interest to solid-state chemists and materials scientists due to their potential use as substrates for high T_c superconductors and for the fabrication of miniature microwave devices [1–3]. These applications are a consequence of their low chemical reactivity and good dielectric properties that are similar to compounds in other $Ba_2LnB'O_6$ series where B' are the common pentavalent cations.

While the properties of the Ba_2LnTaO_6 tantalates are well known, the precise structures within this series of compounds are still unclear. Previous reports using conventional (laboratory) X-ray powder diffraction have indicated that the structures of the largest lanthanides (La^{3+}–Nd^{3+}) are monoclinic, with smaller lanthanides (Eu^{3+}–Tb^{3+}) adopting a tetragonal structure and the smallest lanthanides having cubic symmetry (Dy^{3+}–Lu^{3+} and Y^{3+}) [4–7]. However none of these studies determined the complete structures of these perovskites.

The apparent increase in symmetry of compounds in the series Ba_2LnTaO_6 as the ionic radius of the lanthanide decreases is consistent with an increase of the tolerance factor, t, $t = (r_{Ba} + r_O)/\sqrt{2}(\bar{r}_{(Ln,Ta)} + r_O)$ (r_{Ba} = radius of Ba^{2+}, r_O = radius of O^{2-} and $\bar{r}_{(Ln,Ta)}$ = average radius of the Ln^{3+} and Ta^{5+} cation in the perovskite structure), as the radii of the lanthanide decreases. An increase in the tolerance factor indicates that the volume of the BO_6 octahedron is better matched to the size of the AO_{12} polyhedron reducing the need for the octahedral tilting to accommodate the A-site cation. Since octahedral tilting is responsible for the lowering of the symmetry from cubic, the symmetry tends to increase as the octahedral tilt approaches zero.

A re-examination of the structures of Ba_2LnTaO_6 by Doi and Hinatsu [8] using conventional X-ray diffraction reported that the larger lanthanides (La^{3+}–Tb^{3+}) adopted $P2_1/n$ monoclinic symmetry while the smaller lanthanides (Dy^{3+}–Lu^{3+} and Y^{3+}) adopted $Fm\bar{3}m$ cubic symmetry.

*Corresponding author. Fax: +61 2 9351 3329.
E-mail address: kennedyb@chem.usyd.edu.au (B.J. Kennedy).

0022-4596/$ - see front matter © 2007 Elsevier Inc. All rights reserved.
doi:10.1016/j.jssc.2007.08.009

These workers did not find any evidence suggestive of the intermediate tetragonal structure. However their published lattice parameters appear to show unusual behavior with those tantalates containing lanthanides La^{3+}–Sm^{3+} having lattice parameters where $a>b\approx c/\sqrt{2}$ and those with Ln = Eu^{3+}–Tb^{3+} $a\approx b>c/\sqrt{2}$ which may indicate a phase transition occurs between Ba_2SmTaO_6 and Ba_2EuTaO_6. This suggests the possibility of an intermediate structure. The most likely intermediate structure, as suggested by the earlier work, would be tetragonal and possibly in space group $I4/m$, the most commonly observed tetragonal double perovskite structure. This tetragonal structure was also found in the analogous Ba_2LnNbO_6 (Ln = Eu^{3+}–Tb^{3+}) niobates in our previous studies [9]. In general the niobates and tantalates are expected to exhibit similar structures due to similarities in ionic radii and electronegativity. However it is also possible that an intermediate rhombohedral structure may be formed as is observed for other $Ba_2LnB'O_6$ (B' = Sb^{5+}, Ir^{5+}, Ru^{5+} and Bi^{5+}) [9–12] oxides. Determining which of the two possible intermediate space groups, if any, the tantalate series adopts will provide further insight into why compounds with such similar cations and electrostatic arrangements adopt two different intermediate structures.

A second anomaly is that previous studies often report that when $Ba_2LnB'O_6$ compounds have a monoclinic structure this is usually in space group $I2/m$ rather than $P2_1/n$ as suggested by Doi and Hinatsu [9,12]. The difference between these two monoclinic structures is that in $I2/m$ the single octahedral tilt occurs around the 1 1 0 axis in an out-of-phase fashion (Glazer tilt system $a^-a^-c^0$ [13,14]) while in $P2_1/n$ a second, in-phase tilt around the 0 0 1 axis is also present and the resulting tilt system is described as $a^-a^-c^+$. The diffraction patterns of the two structures are therefore different, with the pattern of a compound in $I2/m$ only displaying R-point superlattice reflections in-addition to the peaks from the parent $Pm\bar{3}m$ perovskite structure. R-point reflections occur in the diffraction patterns of all rock salt ordered double perovskites as a result of the cation ordering. Any out-of-phase tilt that is present will also contribute to the intensity of these reflections. The diffraction patterns of compounds in $P2_1/n$ should also exhibit additional M- and X-point superlattice reflections, as a consequence of the presence of the in-phase tilts and the combination of the in-phase and out-of-phase tilts, respectively. Discriminating between these two monoclinic perovskite structures using powder X-ray diffraction, particularly when employing a relatively weak conventional source rather than a synchrotron, can be difficult. This is because the intensities of the M- and X-point reflections, that are diagnostic of the in-phase tilts, are primarily determined by the positions of the oxygen anions and, as such, are relatively weak in X-ray diffraction particularly in the presence of heavy elements, such as the lanthanides. It should be mentioned that there is also a second contribution to the intensity of M- and X-point superlattice reflections from the displacement of the A-cations from the positions adopted in the $I2/m$ structure. Since the displacement of the A-site cations from this position is typically small the displacement of the oxygen anions is usually the main contributor to the intensity of these superlattice reflections.

We report here part one of a study examining the structures of the series Ba_2LnTaO_6. This paper describes the structures of these compounds at ambient temperature using predominantly synchrotron X-ray diffraction to establish the symmetry of the compounds in this series. The higher resolution and intensity offered by synchrotron X-ray diffraction makes it easier to resolve the splitting of peaks in perovskites, particularly those which may appear to be pseudo-cubic, and to detect the weak superlattice peaks. The study also utilizes neutron diffraction in the case of Ba_2LaTaO_6 to discriminate between the $P2_1/n$ and $I2/m$ space groups. The combination of these two techniques more accurately allows the determination of the sequence of structures adopted by these double perovskites, thus establishing the physicochemical behavior of this series. The second part of this work, which will be published sequentially, arises from unexpected results concerning the structure of Ba_2LaTaO_6. It focuses on the re-examination of the series of phase transition undertaken by both the tantalate and analogous niobate series with changing temperature. Both of these papers provide further insight into the relative stability of rhombohedral and tetragonal symmetry structures in the $Ba_2LnB'O_6$ family of series and increase the understanding of why double perovskites adopt certain symmetries.

2. Experimental

All starting materials were obtained from Aldrich Chemicals. The lanthanide oxides and barium carbonate were dried prior to use by heating overnight at 1000 and 100 °C, respectively. Samples of Ba_2LnTaO_6 (Ln = La^{3+}, Pr^{3+}–Lu^{3+} and Y^{3+}) were prepared from stoichiometric mixtures of $BaCO_3$, Ta_2O_5 and, in the majority of cases, Ln_2O_3. Samples with Ln = Pr^{3+} and Tb^{3+} were prepared using Pr_6O_{11} and Tb_4O_7. The appropriate starting oxides were finely ground, as acetone slurry, and after drying were initially heated at 1200 °C for 12 h. The oxides were then reground and pressed into pellets before heating at 1300 °C for 72 h with subsequent heating as required at 1350 °C for 48 h and at 1400 °C for 60 h to obtain products with the maximum purity. The samples were cooled in the furnace to 300 °C and then removed. In all cases, samples were reground and repelleted after heating periods of either 24 or 48 h.

The reactions were monitored by powder X-ray diffraction using Cu$K\alpha$ radiation on a Shimadzu X-6000 Diffractometer. Synchrotron X-ray diffraction data were recorded on the Debye Scherrer Diffractometer at the Australian National Beamline Facility, Beamline 20B at the Photon Factory, Tsukuba, Japan [15]. The samples were housed in 0.3 mm capillaries that were continuously

rotated during measurement to improve statistical averaging and to reduce the effects of preferred orientation. Data were collected at ambient temperature using three image plates as detectors covering the range of approximately $5<2\theta<125^\circ$ with a step size of 0.01° and a wavelength of either 0.80088(1) or 0.80123(1) Å.

Neutron powder diffraction patterns were collected for Ba_2LaTaO_6 at ambient temperature and at 36 K using the high-resolution diffractometer, HRPD, at the HIFAR reactor operated by the Australian Nuclear Science and Technology Organization (ANSTO), Lucas Heights, Australia using a wavelength of 1.4918(1) Å over a range of 10–150° (2θ angles) with a step size of 0.05° [16]. The sample was held in a 12 mm vanadium can that was continuously rotated during the measurements. Neutron diffraction patterns were also obtained from the medium resolution neutron diffractometer (MRPD) at the same facility using a cryofurnace over the range of 15–500 K with a usual step of 50 K between each pattern [17]. Data were collected at a wavelength of 1.665(1) Å from 8° to 138° (2θ angles) with a step size of 0.1°.

Refinements of the crystal structures were performed with the program RIETICA [18]. The diffraction peaks were described by a pseudo-Voight function using a Howard asymmetry correction where necessary [18]. For neutron diffraction patterns the background was calculated using a six-parameter polynomial while for the X-ray patterns the background was estimated from interpolation between up to 40 selected points.

Scanning electron microscopy (SEM) and energy dispersive X-ray analysis (EDX) were done using a Phillips XL 30 SEM with a tungsten filament operating at 25 keV and a spot size of 5 μm. The EDX operation and data analysis were performed using the DX-4eDX ZAF operating system.

To verify the symmetry and geometry of the crystal structure of Ba_2LaTaO_6 we performed first principles calculations within the framework of density functional theory (DFT). We used the projector augmented wave method (PAW) [19,20], as implemented in the Vienna *ab initio* simulation package (VASP) [21,22], with the Perdew—Burke–Ernzerhof (PBE) [23] form of the generalized gradient approximation (GGA). Both atomic positions and unit cell volume and shape were optimized using a plane-wave energy cut-off 500 eV and the Brillouin zone sampling with a $4\times4\times3$ k-point Monkhorst-Pack [24] mesh (24 irreducible k-points). The symmetry unconstrained optimization was carried out using a quasi-Newton algorithm until the Hellmann–Feynman forces were less than 0.001 eV/Å on each atom.

3. Results and discussion

Determining the correct symmetry and space groups for perovskite-type oxides can be far from trivial, and is achieved by careful examination of both splitting of the strongest Bragg reflections to establish the cell metric and the systematic presence and/or absence of the weaker superlattice reflections indicative of cation ordering, octahedral tilting, cation displacement or a combination of these. In this work we have assigned space groups as those with the highest possible symmetry that accounts for all the observed reflections and is in-keeping with the group theoretical analysis of Howard, Kennedy and Woodward [15].

3.1. Determination of the structures of Ba_2LnTaO_6 at room temperature

The majority of the peaks in the synchrotron X-ray powder diffraction patterns in the compounds could be indexed to a primitive cubic structure with $a\sim4.0$ Å, although in the case of the larger lanthanides these peaks were clearly split (see Fig. 1). There were, however, a few weaker peaks that were also observed. The majority of these weaker peaks were readily indexed, to a double cell, as having odd–odd–odd indices indicating them to be R-point reflections indicative of cation order and/or out-of-phase tilting. The only exception to this was that the diffraction patterns for those compounds containing Gd^{3+} and the smaller lanthanides Dy^{3+}–Lu^{3+} displayed a number of weak additional peaks. These peaks could not be indexed to either M- or X-point reflections but rather were due to the presence of a small amount of Ln_2O_3. Both Ba_2GdTaO_6 and Ba_2DyTaO_6 contained trace quantities of this impurity and it was not possible, by Rietveld refinement, to quantify the amount of this second phase present in the sample while the other compounds were found to contain approximately 1 wt% Ln_2O_3.

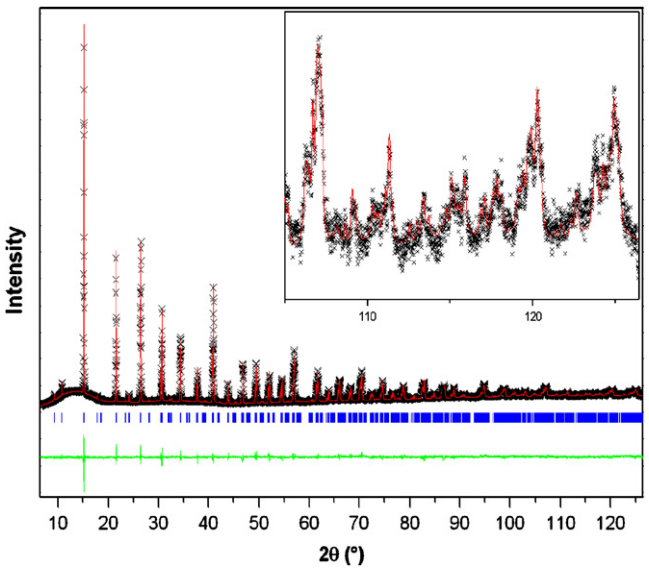

Fig. 1. Synchrotron X-ray diffraction pattern of Ba_2PrTaO_6. The inset shows both the high quality of data collected out to high 2θ and the peak splitting clearly indicating that the symmetry of this structure is lower than cubic. The crosses, upper continuous line and lower continuous line represent the observed intensity, the calculated intensity and the difference between the two, respectively. The vertical markers represent the Bragg reflection markers.

That the diffraction patterns of the $BaLnTaO_6$ oxides contained only *R*-point super lattice reflections and not *M*- or *X*-point reflections, showed according to the group theoretical analysis of Howard et al. [25], that only five double perovskite space group are possible; $P\bar{1}$ triclinic (tilt system $a^-b^-c^-$), $I2/m$ monoclinic ($a^-a^-c^0$), $R\bar{3}$ rhombohedral ($a^-a^-a^-$), $I4/m$ tetragonal ($a^0a^0c^-$) and $Fm\bar{3}m$ cubic ($a^0a^0a^0$). The splitting of the diffraction peaks in Ba_2PrTaO_6 and Ba_2NdTaO_6 is consistent with monoclinic symmetry as previously reported. This can be seen from the splitting of the peaks that would correspond to the (4 4 4) and (8 0 0) peaks in the cubic double perovskite structure into a triplet and doublet, respectively (see Fig. 2). The absence of any *M*- or *X*-point superlattice reflections suggests that the previous conclusion by Doi and Hinatsu [8] that these monoclinic compounds have space group $P2_1/n$ is incorrect. Rather we conclude that these compounds are in space group $I2/m$ consistent with other series in the $Ba_2LnB'O_6$ family and particularly the analogous niobates [9]. At this point that the diffraction pattern of Ba_2LaTaO_6 suggests a more complicated structure at room temperature than is the case for Ba_2PrTaO_6 and Ba_2NdTaO_6, and this point will be returned to later.

The diffraction patterns of the Ba_2LnTaO_6 (Ln = Eu^{3+}–Dy^{3+}) tantalates lack any apparent splitting of the (4 4 4) peak near $2\theta = 38^\circ$ which appears as a single peak, but the cubic (8 0 0) peak near $2\theta = 44^\circ$ remains as a doublet. Critically, there is a reversal in the relative intensity of the two peaks near $2\theta = 44^\circ$ compared to that found in the monoclinic structure (see Fig. 2). This is consistent with a change in symmetry to $I4/m$. The diffraction pattern of Ba_2SmTaO_6 was poorly fitted by models in either monoclinic, $I2/m$, or tetragonal, $I4/m$, symmetry. However, a good fit was obtained using a two phase, monoclinic and tetragonal, model (R_p and R_{wp} of 4.5% and 5.6%, respectively, for the first histogram of the two phase model as opposed to 5.6% and 7.1 % for $I2/m$ symmetry and 12.3% and 15.4% for $I4/m$ symmetry) where the monoclinic phase was the more abundant phase. This is consistent with the phase transition between $I2/m$ and $I4/m$ being first order as required by the group theoretical analysis of Howard et al. [25]. As a consequence of the similarity of the equivalent primitive volume of the two phases there was considerable overlap of the reflections from the two phases. Therefore the refinements were carefully monitored to avoid false minimums and to ensure the resulting structures were chemically reasonable.

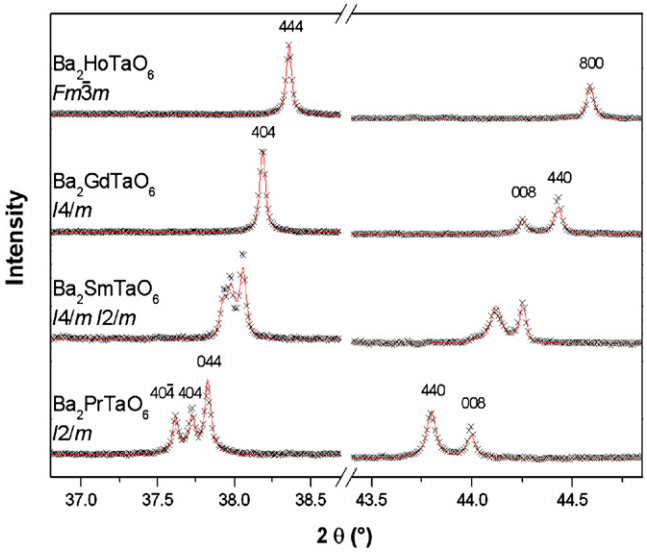

Fig. 2. Selected regions of diffraction pattern for several of the tantalate compounds illustrating the various symmetries adopted in this series. The regions selected are those that correspond to the (4 4 4) and (8 0 0) peak in the cubic structure. The format is the same as for Fig. 1.

For the smallest lanthanides, Ho^{3+}- Lu^{3+} and for Y^{3+}, there is no evidence for any splitting of the reflections in the synchrotron X-ray diffraction patterns indicating that these structures adopt cubic, $Fm\bar{3}m$, symmetry (see Fig. 2). Interesting the *R*-point reflections for those compounds from Er^{3+} to Lu^{3+} are weak or not observed. This could be interpreted as showing that the two *B*-site cations are not ordered in these tantalates. However, given there is no tilting of the BO_6 octahedra in the cubic structure, the intensity of the *R*-point reflections depends on the contrast between the scattering from the lanthanide and tantalum cations. For the heavier lanthanides, Er^{3+}–Lu^{3+}, a difference of three or less electrons between the Ln^{3+} and Ta^{5+} cations results in poor contrast in X-ray diffraction. Therefore the *R*-point reflections are expected to be very weak. By comparison, the difference in the number of electrons between Y^{3+} and Ta^{5+} is 32, resulting in strong contrast between the Y^{3+} and Ta^{5+} using X-ray diffraction. Consequently the *R*-point reflections in Ba_2YTaO_6 are much more intense than observed for the other cubic tantalates. This remarkable difference in the intensity of the *R*-point reflections in Ba_2YTaO_6 and the other tantalates is a powerful reminder that the majority of the intensity in the *R*-point reflections of double perovskites, using X-ray diffraction, is due to cation ordering and not octahedral tilting. Obviously the tantalates adopting the cubic double perovskite structure do not have any octahedral tilting.

3.2. Structure of Ba_2LaTaO_6

The diffraction pattern of Ba_2LaTaO_6 was unique in the Ba_2LnTaO_6 series in that it could not be satisfactorily fitted with either single or multi-phase models using monoclinic, tetragonal or cubic symmetry (see Fig. 3). As found for the other tantalates we failed to observe any intensity associated with the *M*- or *X*-point superlattice reflections. The only other possible space groups, adopted by double perovskites that do not have in-phase tilts are, $P\bar{1}$ and $R\bar{3}$. However the diffraction pattern was not consistent with a single-phase model in either of these space groups. Rather, a two-phase model using a combination of $I2/m$ monoclinic and $R\bar{3}$ rhombohedral symmetries provided the best fit to

the diffraction pattern (R_p and R_{wp} for the first histogram of 4.2% and 5.6%, respectively). This model also accounted for the splitting of the peaks in the diffraction pattern; for example the cubic (4 4 4) reflection appears as five peaks; a triplet of peaks from the monoclinic phase and a doublet of peaks from the rhombohedral phase, and the cubic (8 0 0) reflection is split into three peaks; a doublet of peaks from the monoclinic phase and a single peak from the rhombohedral phase (see Fig. 3). Since this compound adopts a different structure to the other tantalates, and is two phases at room temperature, a combination of SEM and EDX was used to examine the purity of this sample to determine if this unusual behavior was caused by sample inhomogeneities. Backscattered images of the sample did not show evidence of phase segregation (see Fig. 4) and the chemical composition determined by EDX did not vary significantly over the 15 spots examined, each giving a chemical composition in excellent agreement with the expected stoichiometry. Therefore, it is unlikely that co-existence of the monoclinic and rhombohedral phases in this sample is caused by composition inhomogeneity. Rather, as described for Ba_2SmTaO_6, the presence of the two phases is thought to indicate that the sample at room temperature is partway through a discontinuous phase transition. This is consistent with Landau theory that requires the $I2/m$ to $R\bar{3}$ transition to be first order [25]. No other combination of phases can account for the splitting in the diffraction pattern of Ba_2LaTaO_6 unless at least one of these is a triclinic $P\bar{1}$ phase that is rare [27].

To confirm the phase composition of Ba_2LaTaO_6 high-resolution neutron diffraction of this compound was undertaken. A pattern at 36 K was collected initially and featured clear M- and X-point reflections (see Fig. 5). Additionally the splitting of the peaks was consistent with monoclinic symmetry. This suggests that at 36 K Ba_2LaTaO_6 adopts

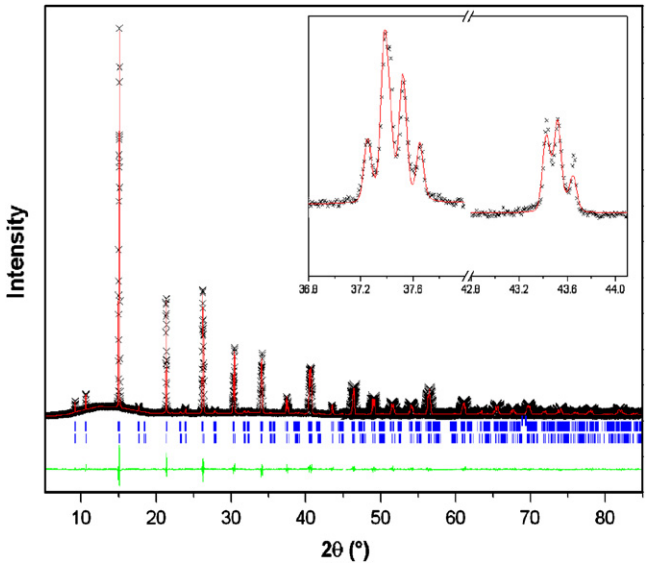

Fig. 3. Synchrotron X-ray diffraction pattern of Ba_2LaTaO_6. The inset is of the basic (4 4 4) and (8 0 0) reflection that are split into five and three peaks, respectively. The format is the same as for Fig. 1 with the upper and lower Bragg reflections corresponding to the $I2/m$ and $R\bar{3}$ structures, respectively.

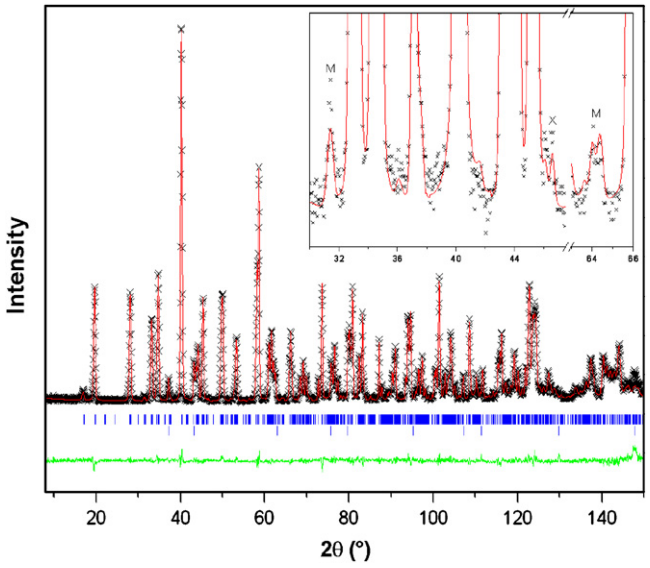

Fig. 5. Neutron diffraction pattern of Ba_2LaTaO_6 obtained at 36 K fitted to $P2_1/n$ symmetry. The insert indicates the most intense M- and X-point superlattice reflections that are indicative that this monoclinic structure adopts $P2_1/n$ symmetry. The format is the same as for Fig. 1. The upper and lower vertical markers represent the Bragg reflections of Ba_2LaTaO_6 and the aluminum cap on the sample can, respectively. The poor fit at approximately 148° is due to texture in the Al cap.

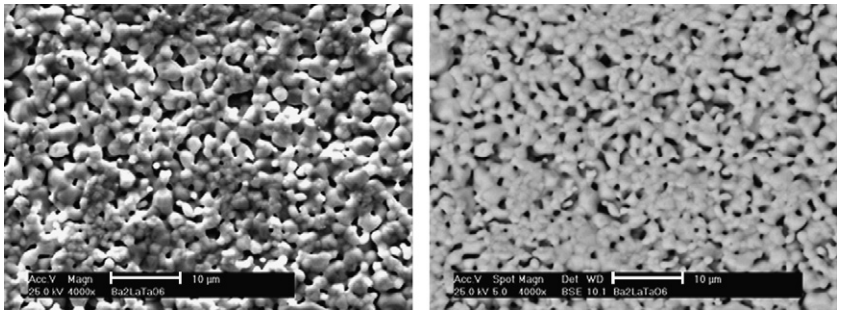

Fig. 4. Secondary electron (left) and backscattered electron (right) images of Ba_2LaTaO_6. The lack of contrast in the backscattered electron image is consistent with a homogeneous sample.

$P2_1/n$ symmetry, and an excellent fit was obtained using such a model. This represents, to the best of our knowledge, the first time a compound in the series $Ba_2LnB'O_6$, where B' is a pentavalent cation, has been shown by neutron diffraction to exist in space group $P2_1/n$. While other studies, most significantly the work of Doi and Hinatsu [8] and Henmi and co-workers [28], have suggested that compounds in this family do adopt $P2_1/n$ these assignments have all relied on powder X-ray diffraction measurements. The rationale behind their assignment appears to be that $P2_1/n$ is the most commonly observed space group for double perovskites with monoclinic symmetry rather than reliance on the observance of the diagnostic super-lattice reflections. In the present case, even in neutron diffraction patterns, the *M*- and *X*-point super-lattice reflections are weak (see Fig. 5) suggesting that these peaks would, most likely, not be observed except in the highest quality synchrotron X-ray powder diffraction patterns.

To provide further confirmation that the low temperature structure of Ba_2LaTaO_6 adopts $P2_1/n$ symmetry a DFT calculation was carried out to determine the minimum energy structure of the compound at 0 K. Even though no symmetry constraints were imposed, geometry optimization smoothly converged to the unit cell with virtually monoclinic metrics ($a = 6.2076$ Å, $b = 6.1472$ Å, $c = 8.6897$ Å, $\alpha = 90.000°$, $\beta = 90.522°$, $\gamma = 89.999°$). Examination of the atomic coordinates revealed that crystal structure could be described using $P2_1/n$ space group within tolerance 0.01 Å.

Having determined the low temperature structure of Ba_2LaTaO_6, a room temperature neutron diffraction pattern was obtained. It retained splitting consistent with monoclinic symmetry but did not have any observable reflections indicative of in-phase tilting indicating that the structure at this temperature was in $I2/m$. Attempts to fit the pattern with a model using a mixture of rhombohedral and monoclinic phases as required for the synchrotron X-ray diffraction pattern did not result in any significant improvement in the quality of the fit and refinements using such a two-phase model suggested little or no rhombohedral phase was present. That the synchrotron X-ray diffraction pattern indicated a mixture of phases at ambient temperature while neutron diffraction indicated that only the single-$I2/m$ phase was present is somewhat puzzling and is a significant inconsistency. It is most likely explained by the histories of the neutron and X-ray samples being different because they were prepared separately. The most significant difference between the way in which the samples were prepared would appear to be that the neutron sample needed to be heated for an additional 24 h at 1300 °C and that the neutron sample was cooled to 36 K for three days for collection of the low temperature neutron diffraction pattern before the room temperature pattern was obtained. Presumably one of these two differences is responsible for the difference in the phase composition at room temperature.

To determine the $P2_1/n$ to $I2/m$ transition temperature and to confirm that the rhombohedral structure does indeed form at some higher temperature additional neutron diffraction patterns were collected over the range of 15–500 K using the MRPD. The $P2_1/n$ structure persisted up to 100 K; the pattern collected at 150 K showed no evidence for any *M*- or *X*-point reflections demonstrating that the structure at this temperature is $I2/m$. A plot of tilt angle versus temperature (see Fig. 6) shows that the out-of-phase tilt angle around the 1 1 0 axis does not change significantly during the phase transition between the two monoclinic phases while the in-phase tilt around the 0 0 1 axis in the $P2_1/n$ structure decreases towards zero as the phase transition approaches. These tilt angles have been calculated using the formulas derived by Howard et al. [29] and have been presented for the smaller TaO_6 octahedron.

The neutron diffraction patterns collected at 450 and 500 K revealed the coexistence of the rhombohedral and monoclinic, $I2/m$, phases. That the rhombohedral phase exists in the sample used for neutron diffraction, shows that the rhombohedral structure in Ba_2LaTaO_6 is the stable structure above room temperature. The full sequence of phase transitions for Ba_2LaTaO_6 is therefore from $P2_1/n$ to $I2/m$ to $R\bar{3}$ and, presumably by analogy with other $Ba_2LnB'O_6$ compounds, to $Fm\bar{3}m$ at higher temperatures.

3.3. Crystal chemistry of Ba_2LnTaO_6

Atomic positions and bond distances for selected members of the tantalate series are recorded in Table 1 and 2. As the size of the lanthanide ion decreases the Ba–O bond distances decrease resulting in the bond valency of the Ba^{2+} cation becoming closer to the ideal value of two

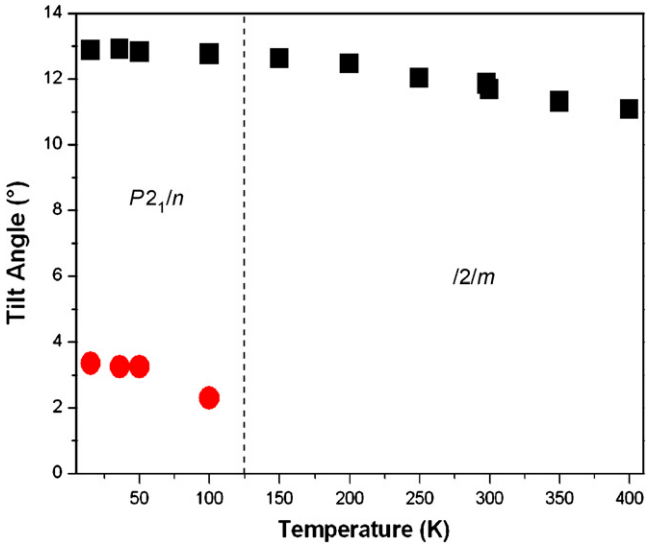

Fig. 6. Tilt angles calculated for Ba_2LaTaO_6 from neutron diffraction measurements. The tilt angle for the monoclinic phase is not shown between 400 and 500 K as this region is two phase, which due to limitations in the resolution of the data, means that it is not possible to calculate accurate tilt angles.

Table 1
Lattice parameters and atomic positions for selected members of Ba_2LnTaO_6 using neutron diffraction data where available

Compound	Ba_2LaTaO_6			Ba_2EuTaO_6	Ba_2YTaO_6
	36 K	Ambient temperature	500 K		
Space Group	$P2_1/n$	$I2/m$	$R\bar{3}$	$I4/m$	$Fm\bar{3}m$
a (Å)	6.14396(9)	6.14860(13)	6.10092(35)	6.00518(6)	8.43539(4)
b (Å)	6.08390(10)	6.09643(13)	$=a$	$=b$	$=a$
c (Å)	8.59860(13)	8.61090(17)	$=a$	8.53106(9)	$=a$
α(°)	90	90	60.2813(52)	90	90
β(°)	90.5178(8)	90.3447(11)	$=\alpha$	90	90
γ(°)	90	90	$=\alpha$	90	90
Ba	4*e* (*x*,*y*,*z*)	4*i* (*x*,0,*z*)	2*c* (*x*,*x*,*x*)	4*d* (0,$\frac{1}{2}$,$\frac{1}{4}$)	8*c* ($\frac{1}{4}$,$\frac{1}{4}$,$\frac{1}{4}$)
x	0.5058(3)	0.5050(5)	0.2526(6)	0	$\frac{1}{4}$
y	−0.0091(5)	0	$=x$	$\frac{1}{2}$	$\frac{1}{4}$
z	0.2477(2)	0.2470(4)	$=x$	$\frac{1}{4}$	$\frac{1}{4}$
B (Å^2)	0.15(2)	0.78(2)	1.60(5)	0.74(1)	0.73(1)
Ln	2*a* (0,0,0)	2*a* (0,0,0)	1*a* (0,0,0)	2*a* (0,0,0)	4*a* (0,0,0)
B (Å^2)	0.16(2)	0.44(3)	1.10(3)	0.36(1)	0.44(1)
Ta	2*b* (0,0,$\frac{1}{2}$)	2*d* (0,0,$\frac{1}{2}$)	1*b* ($\frac{1}{2}$,$\frac{1}{2}$,$\frac{1}{2}$)	2*b* (0,0,$\frac{1}{2}$)	4*b* ($\frac{1}{2}$,$\frac{1}{2}$,$\frac{1}{2}$)
B (Å^2)	0.18(3)	0.38(3)	1.10(3)	0.36(1)	0.44 (1)
O1	4*e* (*x*,*y*,*z*)	4*i* (*x*,0,*z*)	6*f* (*x*,*y*,*z*)	4*e* (0,0,*z*)	24*e* (*x*,0,0)
x	0.0699(3)	0.0642(4)	0.2241(4)	0	0.2646(5)
y	0.0048(5)	0	0.3173(4)	0	0
z	0.2727(2)	0.2721(3)	0.7285(8)	0.2678(24)	0
B (Å^2)	0.53(2)	1.15(4)	2.61(4)	2.08(21)	1.28(5)
O2	4*e* (*x*,*y*,*z*)	8*j* (*x*,*y*,*z*)		8*h* (*x*,*y*,0)	
x	0.2621(3)	0.2741(2)		0.2817(37)	
y	0.2829(4)	0.2690(3)		0.2474(35)	
z	−0.0362(3)	−0.0343(2)		0	
B (Å^2)	0.63(4)	1.47(3)		2.10(21)	
O3	4*e* (*x*,*y*,*z*)				
x	0.2867(3)				
y	0.7444(3)				
z	−0.0382(3)				
B (Å^2)	0.50(4)				
R_p %	4.0	4.8	4.1	5.2	6.0
R_{wp} %	4.9	5.8	4.9	6.1	6.6
R_{exp} %	3.0	3.4	3.1	0.5	0.4

[30]. This reduces the need for octahedral tilting and therefore results in a higher symmetry structure.

The bonds lengths and bond valence sums provide an insight into the compromise in bonding required when cations which do not have an ideal size ratio are incorporated into a double perovskite structure. We find that in Ba_2LnTaO_6 the Ln^{3+} ions are consistently over-bonded with the Ln–O bond lengths being significantly shorter than would be expected based on their ionic radii [26]. This is clearly illustrated by the mean bond valence sum (BVS) of the lanthanides being 3.5(2) across the series. This overbonding of the lanthanide cations is consistent with similar over-bonding observed for the Ba_2LnNbO_6 series in our previous study [9] and is thus not unexpected. The overbonding is most likely caused by the large mismatch in size between the transition metals on the *B*-site and the larger lanthanide cations that more commonly occupy the *A*-sites in perovskites. In both series it appears that the compromise between the bonding requirements of the Ba^{2+} and Ln^{3+} cations results in the underbonding of the Ba^{2+} cations and the over-bonding of the Ln^{3+} cations.

The mean Ta–O bond length, across all the structures studied using powder neutron diffraction is 2.00(1) Å which is noticeably shorter than 2.04 Å, the expected bond distance based on the tabulated ionic radii [26]. The mean BVS is 4.8(2) that are slightly lower than the expected value of 5 for Ta^{5+}. That the BVS is consistently under the expected value despite the shorter than expected Ta–O bond length is puzzling but consistent with previous observations for the Nb^{5+} cations in the analogous Ba_2LnNbO_6 compounds [9]. This discrepancy may warrant further investigation.

The sequence of phase transitions, from lower to higher symmetry with decreasing ionic radii of the lanthanides (see Fig. 7), established for the series Ba_2LnTaO_6 does not fit with the series of phase transitions reported by Doi and Hinatsu [8]. Where they reported a phase transition directly

Table 2
Bond lengths and bond valence sums (BVS) for selected members of Ba_2LnTaO_6

Compound	Ba–O			Ln–O		Ta–O	
	Bond length (Å)		BVS	Bond length (Å)	BVS	Bond length (Å)	BVS
Ba_2LaTaO_6 36K	1 × 2.690(1) 1 × 2.740(2) 1 × 2.788(2) 1 × 2.857(2) 1 × 2.891(1) 1 × 2.999(3)	1 × 3.166(3) 1 × 3.170(2) 1 × 3.246(2) 1 × 3.360(2) 1 × 3.454(2) 1 × 3.472(2)	1.86	2 × 2.380 (2) 2 × 2.379 (2) 2 × 2.375 (2)	3.44	2 × 2.005 (2) 2 × 1.993 (2) 2 × 2.007 (2)	4.81
Ba_2LaTaO_6 ambient temperature	1 × 2.720(4) 2 × 2.814(3) 2 × 2.869(3) 2 × 30820(6)	2 × 3.245(3) 2 × 3.332(3) 1 × 3.444(4)	1.76	2 × 2.374 (2) 4 × 2.371 (2)	3.50	2 × 2.004 (2) 4 × 1.999 (2)	4.82
Ba_2LaTaO_6 500 K	3 × 2.785(2) 3 × 3.030(8)	3 × 3.106(8) 3 × 3.355(2)	1.69	6 × 2.358 (3)	3.63	6 × 2.003 (3)	4.80
Ba_2EuTaO_6	4 × 2.91(1) 4 × 3.006(1) 4 × 3.12 (1)		1.76	2 × 2.29 (2) 4 × 2.25 (3)	3.63	2 × 1.98 (2) 4 × 2.00 (2)	4.88
Ba_2YTaO_6	12 × 2.9849(2)		1.83	6 × 2.232 (4)	3.33	6 × 1.986 (4)	5.02

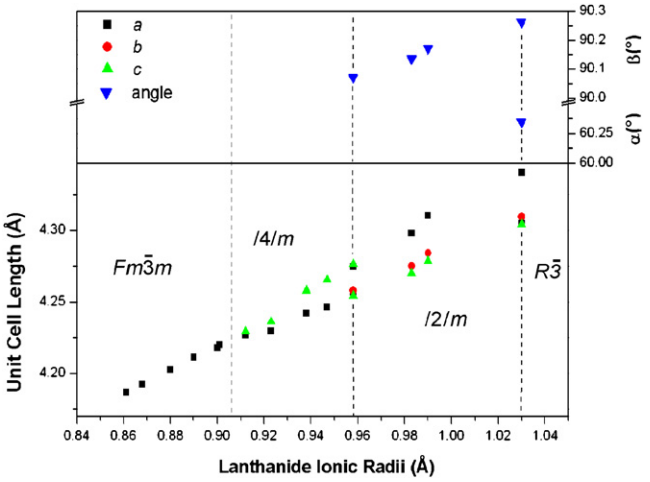

Fig. 7. Unit cell parameters for Ba_2LnTaO_6 showing the increase in symmetry of the various members of this series with decreasing lanthanide ionic radius. The unit cell lengths have been reduced to the same size as the primitive cubic perovskite.

from $P2_1/n$ (tilt system $a^-a^-c^+$) monoclinic to $Fm\bar{3}m$ ($a^0a^0a^0$) cubic we found that the sequence is from monoclinic $I2/m$ ($a^-a^-c^0$) to tetragonal $I4/m$ ($a^0a^0c^-$) and then to $Fm\bar{3}m$ symmetry with decreasing ionic radii of the lanthanide. We also find that the $P2_1/n$ phase exists in Ba_2LaTaO_6 but only at low, <100 K, temperatures.

The findings of this study are more consistent with work published prior to Doi and Hinatsu and in particular the work of Evdokimov and Men'shenina [4], the only discrepancies being they describe Ba_2DyTaO_6 as being cubic and that they did not detect the co-existence of the rhombohedral phase in Ba_2LaTaO_6. This highlights the advantage of the higher resolution synchrotron X-ray diffraction measurements reported here, in that it revealed the small splitting of diagnostic peaks in Ba_2DyTaO_6 indicative of tetragonal symmetry.

The preference of the majority of the tantalate series for a tetragonal structure intermediate between the monoclinic and cubic end-members is similar to that seen in the analogous niobate and molybdate series [9,31] which also adopt tetragonal symmetry and is in contrast to that of the other series in the $Ba_2LnB'O_6$ family which, as previously noted, adopt rhombohedral symmetry. Since both Nb^{5+} and Ta^{5+} have a d^0 configuration this supports the argument previously suggested by our group based on the work of Woodward [32] that in those compounds where the *B*-site cations contain only a few *d*-electrons the structure with B–O–B' bond angles closest to 180° will be favored to strengthen the π-bonding present in these structures. In this case that is the tetragonal structure.

A recent publication by Fu et al. [33] has questioned our conclusion that π-bonding can play a significant role in determining which intermediate symmetry ($R\bar{3}$ or $I4/m$) is adopted by compounds in the $Ba_2LnB'O_6$ family. These authors suggest that differences in the electronegativity of the second *B*-site cations are responsible for the difference in symmetry. Those oxides containing the most electronegative cations ($B' = Ru^{5+}$, Ir^{5+}, Sb^{5+} and Bi^{5+}) adopt rhombohedral symmetry and those containing the less electronegative cations ($B' = Nb^{5+}$, Ta^{5+} and Mo^{5+}) have tetragonal symmetry [33,34]. Fu et al. [33] correctly pointed out that early attempts to quantify electronegativity have often been incomplete, as they did not account for different oxidation states or co-ordination environments. As a result of this and limitations in the method used to determine the Pauling [35] scale of electronegativity it does

not accurately reflect the chemical behaviour of the various elements.

The electronegativity values referred to in our initial paper [9] were those presented in the recent work by Li and Xue [36]. This work addresses many of the criticisms of the Pauling scale including the violation of the so-called Si rule [37] and electronegativities in various oxidation states and co-ordination environments were determined. This more comprehensive approach to estimating electronegativities uses a similar approach to the Allred–Rochow scale, acknowledged by Fu et al. [33] as a reasonable set of values. However this series is updated with the more accurate ionic radii determined by Shannon [26] and uses ionization energy to determine effective nuclear charge. This is therefore the most complete and accurate electronegativity scale currently available. The electronegativities derived by Li and Xue provide a comparison between elements in different parts of the periodic table, such as the transition metals, e.g. Mo^{5+} and main group metals such as Sb^{5+} and Bi^{5+}. The values of Li and Xue [36] show that Mo^{5+} is more electronegative than either Bi^{5+} and Sb^{5+} ($\chi_i = 2.006$ for Mo^{5+} c.f. to 1.895 and 1.971 for Bi^{5+} and Sb^{5+}, respectively) while Ta^{5+} and Nb^{5+} have similar electronegativities (1.925 and 1.862) to Bi^{5+}. In the series $Ba_2LnB'O_6$ where $B'^{5+} = Ta^{5+}$, Nb^{5+} or Mo^{5+} the intermediate structure is tetragonal and for $B' = Bi^{5+}$ or Sb^{5+} rhombohedral symmetry is adopted. Even if the electronegativity values determined by Xue and Li [36] are not absolutely correct, the electronegativities of the B' cations are not a sufficiently discriminating gauge of which intermediate symmetry is adopted in the case of the $Ba_2LnB'O_6$ perovskites.

Fu et al. [33] questioned two facets of the π-bonding model that we suggest is important in determining between rhombohedral and tetragonal symmetries. The first of these is why the d^3 (Ru^{5+}) and d^4 (Ir^{5+}) double perovskites do not adopt tetragonal symmetry if the π-bonding hypothesis is correct. As we previously noted there appears to be a boundary in the stability of the tetragonal and rhombohedral structures being between d^1 and d^3. The positioning of the boundary is consistent with the calculations of Woodward [32] on ABO_3 perovskites that showed the maximum stability of the structure favored by π-bonding was for those perovskites that either had d^1 or d^2 configurations. For those compounds containing B-cations with more than two d-electrons the occupancy of the π^* orbitals leads to a destabilization of the π-bonding thus favoring the alternate structure. Fu et al. [33] also questioned the capability of lanthanide cations to participate in π-bonding in these structures and suggested that the nature of any π-bonding present in the $Ba_2LnB'O_6$ compounds, where B' is Nb^{5+}, Ta^{5+} and Mo^{5+}, would be different than the type observed in ABO_3 perovskites. However recent theoretical calculations [38,39] indicate that lanthanides are capable of forming π-bonds with oxygen anions predominantly through their 5d orbitals. Since lanthanides do form π-bonds it seems reasonable to conclude that it is also likely that such π-bonds will be present in the $Ba_2LnB'O_6$ series, as required by our hypothesis, and thus the presence of straight i.e. $\sim 180^\circ$ Ln–O–B' bond angles will be important in stabilizing alternate structures where π-bonding is significant. Since π-bonds in lanthanides tend to be weaker than in transition metals the effect of having two B-site cations with significantly different π-bonding strengths on the preferred structure is unclear and is worthy of further investigation.

We do not dispute that electronegativities are an important gauge in distinguishing between these two competing structures but contend that π-bonding interactions will also be significant when the B' cation has a small number of d-electrons e.g. Nb^{5+}, Ta^{5+} and Mo^{5+} and this favors a tetragonal structure if all other factors are equal as appears to be the case in the $Ba_2LnB'O_6$ oxides.

That Ba_2LaTaO_6 exhibits a rhombohedral structure is surprising. La^{3+} is different from the lanthanides known to adopt tetragonal symmetry (Sm^{3+}–Dy^{3+}) in the tantalates in two ways. La^{3+} is the largest of the trivalent lanthanide cations and, unlike the other lanthanides has no f-electrons. Which of these two factors is responsible for stabilizing the rhombohedral structure of Ba_2LaTaO_6 is unclear. Similarly, whether Ba_2LaNbO_6 and other members of the tantalate and niobate series for which the symmetry of the intermediate phase is yet to be established adopt tetragonal or rhombohedral structure is uncertain. Studies using synchrotron X-ray powder diffraction aimed at determining this will be reported in the second part of this work. That this additional effect is present is a reminder that there are a number of factors that affect the relative stability of various perovskite structures such as electrostatic arrangement (i.e. what charges the various cations have), electronegativity, π-bonding and ionic radii and that it is simplistic to assign all variations in symmetry to differences in one of these.

4. Conclusion

This study has examined the structures of 14 members of Ba_2LnTaO_6 at room temperature using synchrotron X-ray diffraction. The structure across the series changes from $I2/m$ monoclinic to $I4/m$ tetragonal to $Fm\bar{3}m$ cubic symmetry. However Ba_2LaTaO_6 was an exception to this general trend being found by X-ray diffraction to be a mixture of $I2/m$ monoclinic and $R\bar{3}$ rhombohedral symmetry at room temperature. Further analysis of this compound using variable temperature neutron diffraction revealed a sequence of phase transitions from $P2_1/n$ monoclinic to $I2/m$ monoclinic to $R\bar{3}$ rhombohedral symmetry with increasing temperature. The preference for tetragonal symmetry displayed by the majority of compounds studied here, is most likely caused by the presence of π-bonding that favors the structure with the straightest B–O–B' bond angles. At this point the cause of Ba_2LaTaO_6 adopting the rhombohedral structure in preference to the tetragonal structure is

unclear but it is most likely caused by either the large size of the La^{3+} cation or its lack of *f*-electrons.

Acknowledgments

This work has been partially supported by the Australian Research Council. The neutron diffraction work has been supported by the Australian Institute of Nuclear Science and Engineering (AINSE) through the provision of an AINSE Postgraduate Award. The work performed at the Australian National Beamline Facility was supported by the Australian Synchrotron Research Program under the Major National Research Facilities program and was performed with the help of Dr. James Hester. MA would like to thank Prof. G.J. Kearley for fruitful discussions and the Australian Partnership for Advanced Computing (APAC) for allocation of supercomputer time.

Appendix A. Supplementary data

The online version of this article contains additional supplementary data. Please visit doi:10.1016/j.jssc.2007.08.009.

References

[1] S.K. Korchagina, Y.A. Shevchuk, Inorg. Mater. 42 (2006) 64–67.
[2] S.K. Korchagina, N.V. Golubko, Y.A. Shevchuk, V.V. Gagulin, Inorg. Mater. 40 (2006) 1088–1090.
[3] T.G.N. Babu, J. Koshy, J. Solid State Chem. 126 (1996) 202–207.
[4] A.A. Evdokimov, N.F. Men'shenina, Zh. Neorg. Khim. 27 (1982) 2137–2139.
[5] V.U. Wittmann, G. Rauser, S. Kemmler-Sack, Z. Anorg, Allg. Chem. 482 (1981) 143–153.
[6] F.S. Galasso, G.K. Layden, D.E. Flinchbaugh, J. Chem. Phys. 44 (1966) 2703–2707.
[7] P.W. Barnes, M.W. Lufaso, P.M. Woodward, Acta Crystallogr. B 62 (2006) 384–396.
[8] Y. Doi, Y. Hinatsu, J. Phys.: Condens. Matter 2001 (2001) 4191–4202.
[9] P.J. Saines, B.J. Kennedy, M.M. Elcombe, J. Solid State Chem. 180 (2007) 401–409.
[10] W.T. Fu, D.J.W. IJdo, Solid State Commun. 136 (2005) 456–461.
[11] W.T. Fu, D.J.W. IJdo, J. Alloys Compds. 394 (2005) L5–L8.
[12] W.T.A. Harrison, K.P. Reis, A.J. Jacobson, L.F. Schneemeyer, J.V. Waszczak, Chem. Mater. 7 (1995) 2161–2167.
[13] A.M. Glazer, Acta Crystallogr. A 31 (1975) 756–762.
[14] A.M. Glazer, Acta Crystallogr. B 28 (1972) 3384–3392.
[15] T.M. Sabine, B.J. Kennedy, R.F. Garrett, G.J. Foran, D.J. Cookson, J. Appl. Crystallogr. 28 (1995) 513–517.
[16] C.J. Howard, C.J. Ball, R.L. Davis, M.M. Elcombe, Aust. J. Phys. 36 (1983) 507–518.
[17] S.J. Kennedy, Adv. X-Ray Anal. 38 (1995) 35–46.
[18] B.A. Hunter, C.J. Howard, A Computer Program for Rietveld Analysis of X-Ray and Neutron Powder Diffraction Patterns, Lucas Heights Laboratories, 1998.
[19] G. Kresse, D. Joubert, Phys. Rev. B: Condens. Matter 59 (1999) 1758–1775.
[20] P.E. Blöchl, Phys. Rev. A 50 (1994) 17953–17979.
[21] G. Kresse, J. Furthmüller, Phys. Rev. B: Condens. Matter 54 (1996) 11169–11186.
[22] G. Kresse, J. Hafner, Phys. Rev. B: Condens. Matter 558 (1993) 558–561.
[23] J.P. Perdew, K. Burke, M. Ernzerhof, Phys. Rev. Lett. 77 (1996) 3865–3868.
[24] H.J. Monkhorst, J.D. Pack, Phys. Rev. B: Condens. Matter 13 (1976) 5188–5192.
[25] C.J. Howard, B.J. Kennedy, P.M. Woodward, Acta Crystallogr. B 59 (2003) 463–471.
[26] R.D. Shannon, Acta Crystallogr. A 32 (1976) 751–767.
[27] M.W. Lufaso, P.W. Barnes, P.M. Woodward, Acta Crystallogr. B 62 (2006) 397–410.
[28] K. Henmi, Y. Hinatsu, N.M. Masaki, J. Solid State Chem. 148 (1999) 353–360.
[29] B.J. Kennedy, C.J. Howard, K.S. Knight, Z. Zhang, Q. Zhou, Acta Crystallogr. B 62 (2006) 537–546.
[30] I.D. Brown, D. Altermatt, Acta Crystallogr. B 41 (1985) 244–247.
[31] E.J. Cussen, D.R. Lynham, J. Rogers, Chem. Mater. 18 (2006) 2855–2866.
[32] P.M. Woodward, Acta Crystallogr. B 53 (1997) 44–66.
[33] W.T. Fu, S. Akerboom, D.J.W. IJdo, J. Solid State Chem. 180 (2007) 1547–1552.
[34] W.T. Fu, D.J.W. IJdo, J. Solid State Chem. 179 (2006) 1022–1028.
[35] L. Pauling, The Nature of the Chemical Bond and the Structure of Molecules and Crystals: An Introduction to Modern Structural Chemistry, Cornell University Press, Ithaca, 1960.
[36] K. Li, D. Xue, J. Phys. Chem. A 110 (2006) 11332–11337.
[37] L.R. Murphy, T.L. Meek, A.L. Allred, L.C. Allen, J. Phys. Chem. A 104 (2000) 5867–5871.
[38] D.L. Clark, J.C. Gordon, P.J. Hay, R. Poli, Organometallics 24 (2005) 5747–5758.
[39] Z.-J. Wu, S.-Y. Zhang, Chem. Phys. 164 (1992) 197–202.